Impact of preferential vaporization on combustion chamber deposit generation from a gasoline surrogate: A parametric study

A. Roque, J. Hélie, Fabrice Foucher

Impact of preferential vaporization on combustion chamber deposit generation from a gasoline surrogate: a parametric study.

Anthony Roque[a], Jérôme Hélie[b], Fabrice Foucher[a].

[a]Laboratoire Pluridisciplinaire de Recherche en Ingénierie des Systèmes, Mécanique, Energétique (PRISME), Université d'Orléans, 8 Rue Leonard de Vinci, 45072 Orléans Cedex, France.

[b]CPT France SAS (Continental)

Abstract

The effect of injection pressure and impingement-surface temperature on combustion chamber deposit (CCD) inside a constant volume combustion chamber (CVCC) was studied. The CVCC was modified to capture the main characteristics of the spray-wall and film-flame interaction observed in gasoline direct injection (GDI) engines. The measurements were performed at three different injection pressures (30, 100, and 200 bar) and four wall temperatures (353, 393, 433, and 473 K) using a gasoline surrogate (S01) with four components (hexane, iso-octane, toluene, 1-methylnaphthalene), under a global equivalence ratio of one. High speed Schlieren measurements and Mie scattering were used to characterize the spray-wall interaction. Moreover, the influence of the vapor distribution of the heavy and light fractions of a second non-fluorescent surrogate (S02, with similar vaporization behavior and composition to S01) doped with p-difluorobenzene (pDFB) and 1-Methylnaphtalene (1-MN) was analyzed around the impingement region. The fluorescent signal of the traces made it possible to study indirectly the effect of preferential vaporization on the CCD generation. Finally, the CCD build-up rate was determined by a gravimetric method. It was found that regardless of the injection pressure, the maximum production of CCD took place at a wall temperature of 393 K, and that an additional increase in the temperature reduced the build-up rate of CCD. The higher retention of heavy fraction on the impingement region at 353 and 393 K, identified by fluorescence, could not explain by itself the higher production of CCD outside the impingement region.

Keywords: Gasoline direct injection, combustion chamber deposits, preferential vaporization, spray-wall interaction, soot.

Introduction

Stringent legislative regulations on environmental issues combined with high fuel economy requirements have driven GDI engine producers to rethink and improve the main design conceptions of combustion phenomena. Nowadays, the production of GDI engines is growing fast in the U.S. and European markets [1,2]. Nonetheless, one of the main problems presented by GDI engines is the increase in spray-wall interaction due to the increase in injection pressure and downsizing trends. This interaction generates rich regions, where knowledge of the vapor distribution of the light, medium and heavy compounds of multicomponent fuels during the fuel-film formation and before flame-film interaction is crucial, but has not been studied in detail. This phenomenon can be assessed using preferential vaporization (PV) [3], which allows characterizing the evaporation of different components of a multicomponent blend under different operational conditions. Some evidence of the importance of PV was presented in the theoretical description by Senda et al. [4,5] for multicomponent spray vaporization. The authors showed that the more volatile components (light fraction) evaporate earlier around the free spray region, while the less volatile ones (higher boiling point fuels, heavy fraction) evaporate slowly near the piston wall surface. This description was subsequently validated using a numerical simulation in a free spray by Kawano et al. [6] and experimentally by Yoon et al. [7]. Additionally, the physical and chemical properties of the fuel film generated can produce high particulate emissions due to pyrolysis phenomena during the pool fire process [8,9], modifying the nature, structure, and distribution of CCD [10,11]. It is known that fuel blends with a high aromatic content lead to high PN emissions and a faster build-up of CCD [11,12]. A more volatile fuel induces a good mixture formation and combustion and consequently a reduction in particulate emissions [13].

Parametric studies attempting to link soot generation and the CCD mechanism for GDI have also appeared lately. In this regard, Ganeau et al. [14] studied the generation of CCD using commercial gasoline, by exploring two regions: inside and outside the impingement region. Their results showed the presence of two different kinds of formation mechanism, liquid-film-path and soot-path. These mechanisms were initially described by Lepperhoff and Houben [15]. Furthermore, it is important to consider that the build-up of CCD under real engine conditions depends on a complex interaction of

engine parameters (design and operation), fuel additives, and so on [15,16]. Proven mechanisms associated to the reduction of fuel films must be associated to the main drivers in deposit formation. Thus, the main goal of this work is to determine the influence of PV on the soot and CCD around the impingement area, under well-defined conditions. The vaporization process takes place from the start of injection (SOI) to just before the interaction with a premixed flame. The initial combination of Mie scattering and Schlieren techniques gave us valuable information about the liquid and vapor phase during the injection. The PV was studied using two-tracer laser induced fluorescence (2T-LIF) to observe the distribution of the light and heavy species around the impingement region. 2T-LIF is a valuable technique initially developed by Li et al. [17] and recently modified by Lama et al. [18]. Finally, a gravimetric measurement of the CCD production was conducted for around 450 cycles per each condition. The analysis unveiled the significant influence of the heavy fraction vaporization on the deposit build-up rate.

1. Methodology

The gasoline surrogate used for CCD build-up (S01) was a blend of four components (Hexane, toluene, iso-octane and 1-Methylnaphtalene) and was injected using a single-hole solenoid injector. Table 1 shows the volume fraction of each component and its distillation curve is presented in Figure 1. Pitz et al. [19] suggested that the components of a gasoline surrogate should include n-heptane, iso-octane, and toluene. On the other hand, toluene, styrene, m-xylene, and 1-methylnaphthalene (1-MN) can be added to the gasoline surrogate mixture to correctly predict PAH formation [20]. The addition of 1-MN accelerates CCD formation [10,11]. The high content of aromatics in S01 (42.4 vol%) was selected to evaluate the production of soot and CCD even though its vaporization curve cannot match well the distillation curves of the reference commercial gasolines presented in Figure 1.

The tests were carried out inside a CVCC (4.1 liters). Before filling the sphere with gases, a vacuum pump was used to evacuate the vessel and reach a pressure of less than 0.009 bar. An air-fuel mixture for the reactive case or a N_2-fuel mixture for the unreactive case were injected by a thermal flow meter and a Coriolis mass flow meter. The composition of the synthetic air used was 79.1% N_2 and 20.9% O_2. The sphere is equipped with a fan to obtain a homogeneous mixture [21]. The fan was stopped 10 s

before injection and ignition to prevent any perturbation that could disturb the spray penetration and the flame propagation. The temperature of the vessel was fixed for all the tests at 363 K. More details about this experimental setup can be found in [22,23]. Figure 2a shows the internal distribution inside the vessel, where a 50x50x10 mm^3 aluminum plate with an arithmetic average roughness (Ra) of 15 µm was installed. The plate temperature was controlled by a heating and cooling system. The effect of parametric variations of the three injection pressures (P_{inj} of 30, 100, and 200 bar) and four impingement-surface temperatures (T_{wall} of 353, 393, 433, and 473 K) on vaporization and CCD build-up rate was studied. The reactive tests (with spark-ignition) were performed by injecting almost 10.3 mg of fuel regardless of the injection pressure. This quantity was added to the pre-mixture air-fuel at an equivalence ratio (ϕ_{mix}) of 0.96, giving a global equivalence ratio of 1. The premixed air-fuel mixture was ignited by a spark plug located in the topside, 120 mm from the plate, so a flat flame interacted with the fuel film retained on the plate surface, generating pool fires (Figure 2c). A second blend (S02) was used to perform the fluorescence tests, under non-reactive conditions (without ignition and by replacing the oxygen with nitrogen to suppress any O_2 quenching). The change of fuel was necessary for the 2T-LIF, because the reference fuel (S01) presented a high concentration of fluorescent species (i.e. toluene and 1-MN) that promote laser absorption. Lamiel [24] and Roque et al. [23] showed that the two surrogates presented similar vaporization behavior. The composition of S02 is presented in Table 1. pDFB and 1-MN were used as dopants to perform 2T-LIF.

Table 1. Composition of the gasoline surrogates and physical properties of each component (at 298 K and 1.01325 bar)

Component	Chemical formula	First blend (S01) vol%	Second blend (S02) vol%	Density [kg/m3]	N. B. P. [K]	E. V. [kJ/kg]
Hexane	C_6H_{14}	10.3	10.3	656	341.88	365.5
Iso-octane	C_8H_{18}	47.3	78.6	690	372.39	305.5
Toluene	C_7H_8	31.3	-	865	383.79	422.2
1-Methylnaphthalene (1-MN)	$C_{11}H_{10}$	11.1	0.08	1016	517.84	438.8
Dodecane	$C_{12}H_{26}$	-	11.1	745	489.48	361.2
1,4-Difluorobenzene (pDFB)	$C_6H_4F_2$	-	0.032	1162	361.95	313.8

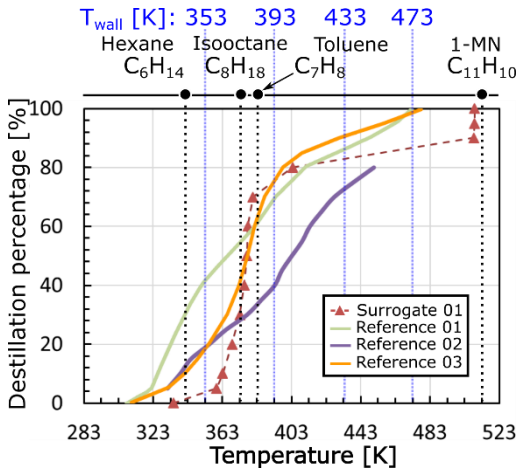

Figure 1. Vaporization curve for the reference fuel (S01), Euro 5 (Ref01 [3]), 91 AI (Ref02 [25]), and premium Tier2 (Ref03 [8]) gasolines. The boiling point of each component in S01 and the wall temperature used in experiments are indicated on the top.

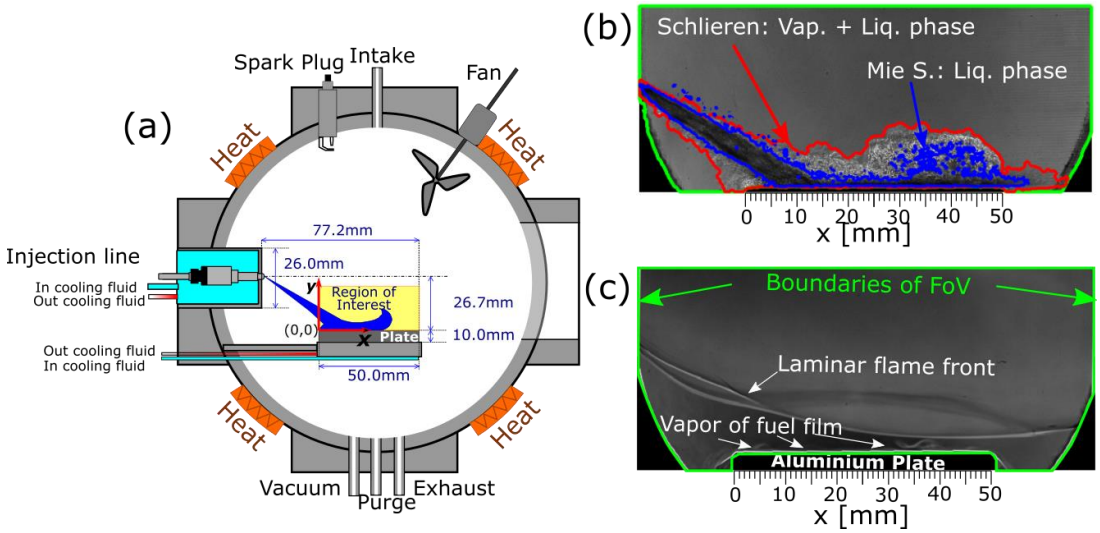

Figure 2. (a) Internal arrangement inside CVV and different moments of the reactive cycle at $P_{inj} = 30\ bar$: (b) injection at $t_{aEIO} = -1.9\ ms$, the contour obtained from the Mie-scattering and Schlieren measurements are shown, and (c) the flame wall interaction at $t_{aEIO} = 38.9\ ms$.

1.1 Mie scattering and Schlieren measurements

The methodology developed by Montonaro et al. [26,27] was used to characterize the impingement. The technique involved the use of two different light sources, one for the Mie scattering and another one for the Schlieren signal. The illumination for each recorded-frame sequence was alternated between Mie and Schlieren signals. The signals of both techniques were acquired at 30 kHz (quasi-simultaneous

measurements) using the same camera. The details of the experimental setup can be found in [22]. This combination of techniques gave an initial approximation of the vaporization process during the impingement, and the right time to start the acquisition process for the 2T-LIF images. The Schlieren images were subjected to an iterative threshold filtering [28], whereas Otsu filtering was applied to Mie-scattering images to determine the boundaries of the liquid and vapor phase as function of time. The areas inside the contours of each signal were used in the analysis. An example of superimposed contours is presented in Figure 2b.

1.2 Two-tracer laser induced fluorescence (2T-LIF)

pDFB and 1-MN were used as tracers, and excited by a Nd-YAG laser at 266 nm. Lama et al. [18] applied these tracers successfully under very well controlled conditions. Some authors have confirmed their applicability even under real engine conditions [29].

The fluorescence signals were recorded simultaneously at two emission ranges using an image doubler (LaVision) and a PI-MAX4 ICCD camera. The range from 275 to 300 nm, and from 320 to 350 nm were selected for the pDFB and 1-MN, respectively. The combination of Asahi-spectra filters ZUS-0300/ZUL-0275, and 20CGA-320 (Newport filter) /ZUS-0350 were used at each channel of the doubler, and for each range. Previous studies [3,18] confirmed that pDFB and 1-MN co-evaporate together with the light-medium and heavy component fractions of a gasoline surrogate, respectively. The non-saturated regime was selected for fluorescence excitation. The acquisition was performed at four different times after the end of injection (aEOI): 4.1; 15.1; 26.1; and 38.1 ms. The first timing (4.1 ms) was selected as a function of the complete vaporization of the liquid phase (obtained by Mie signal). The fourth timing (38.1 ms) was set before wall-flame interaction (Figure 2c), which was determined from cycles running in reactive conditions using Schlieren measurements. Six repetitions were done to analyze the average images. The analyzed 2D maps of pDFB and 1-MN signals were obtained after applying a pixel-to pixel calibration, which corrects the non-uniformity in the laser profile, the differences in the level of intensities, distortions added by the image doubler, and the temperature dependence of the LIF signal. Additional details of the setup and the calibration process can be found in [23].

1.3 Gravimetric test on CCD

Each reactive cycle has a duration of almost 5 minutes and consists of the following main sequence of events: vacuum generation, premixed intake, fuel injection and ignition, and exhaust. After 150 reactive cycles, the aluminum plate was removed and weighed on an analytical balance METTLER AE100S, which presents a minimal sensitivity of 0.1 mg. With this procedure, the build-up rate of deposits was determined by measuring the mass accumulated each 150 up to 450 cycles. The variations in the accumulated mass permitted us to obtain the build-up rate using a linear trend of the data, where the values of R^2 (coefficient of correlation) were higher than 0.92 for all conditions. Due to the long duration of the tests in each condition, the procedure was automated.

2. Results and discussion

2.1 Spray-wall interaction

The initial approximation of the vaporization process was obtained by the combination of Mie scattering and Schlieren measurements. The parameter used to observe the fuel vaporization was the ratio of areas between the Mie scattering signal and the Schlieren measurements (A_{Mie}/A_{Schl}); the results for two P_{inj} are presented in Figure 3. The liquid penetration (L_{Mie}) was added to this Figure and helped us to distinguish the time when the spray liquid phase reached the right edge. The initial ratio values start close to one because the liquid and vapor presented almost the same area at the initial moments of injection. Four different moments were identified: (i) phase I is associated to the free spray traveling to the surface; (ii) phase II corresponds to the passing of the spray tip through the surface; (iii) phase III is the moment when the spray completely covers the impingement region; and (iv) phase IV starts after the EOI. The highest variation of the area ratios took place in phase II and III, and that a higher proportion of liquid reached the surface when the pressure was increased (phase II). This means that the rebounding and splashing after the impact on the plate could have a considerable influence on the vaporization process. The time of direct contact between the spray and the surface is reduced with the pressure rise. There was an increase in vaporization when the injection pressure rose up to 200 bar (phase II and III), which can be attributed to the increase in the impingement plate temperature (T_{wall}). After

the EOI, part of the liquid fuel is vaporized midway between the injector nozzle and the plate surface and next to the plate's right edge.

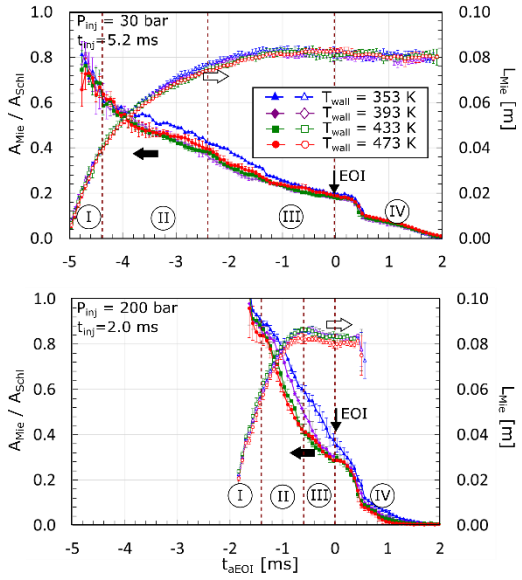

Figure 3. Area ratios as a function of t_{aEOI} were obtained from Mie Scattering and Schlieren measurements during the impingement process at two different injection pressures and four wall temperatures. Average of three injection cycles at each condition.

2.2 Preferential vaporization

Figure 4 shows the values for a reference concentration (C_f) for pDFB and 1-MN at t_{aEOI} equal to 4.1, 15.1, 26.1, and 38.1 ms at $P_{inj} = 200\ bar$. The 2D maps are arranged according to the rise in the wall temperature from left to right, and according to aEOI time from top to bottom. C_f enables the variation in the concentration of each fraction to be compared because its values were obtained from a calibration curve of intensities, for each pixel, obtained at different known fuel concentrations under homogeneous mixture conditions. Each channel can measure the 2D-variation of intensities during the vaporization process of the fuel film. In this way, if the initial concentration of the fuel in the vessel at $\phi = 0.96$ was 0.102 kg/m^3, both maps indicated the same concentration (namely the same proportion between the light and heavy fractions). This is confirmed by the C_f values far away from the plate surface on the maps presented in Figure 4. However, when PV took place, C_f enabled the local variation of one component to be directly compared to the other.

Figure 4a shows that there was a high vaporization of the light fraction around the impingement region at 353 K, and that its vaporization increased with respect to time. Hence, it can be deduced that a considerable quantity of the light fraction was retained on the plate at this temperature. Consequently, the light fraction can be present when flame-film interaction takes place at 38.1 ms. When the temperature was increased to 393 K, the initial higher vaporization of the light fraction was present at 4.1 ms, but at 15.1 ms the vaporization of the heavy fraction overcame the light fraction (comparison with Figure 4b); this is more evident close to the surface. The concentration of the light fraction was considerably reduced when the time increased. Above 433 K, light fraction concentration tended to decrease with time.

The heavy fraction maps presented in Figure 4b show a different behavior to that of the light fraction. It was found that the liquid fraction that reached the surface presented a minimal vaporization at 353 K. When the temperature was increased to 393 K, a considerable increment in the vaporization of the heavy component was observed. The maximum vaporization of the heavy fraction was observed at 433 K; this means that at lower temperatures (353 and 393 K) a considerable quantity of this component was not vaporized. At 473 K, the presence of the fraction was reduced because of the higher rate of vaporization; additionally, the creation of thermal convective flows can improve the mixing and vaporization process. Similar trends were found for the other injection pressures. Therefore, the main driver in the final composition of the fuel film was the wall temperature.

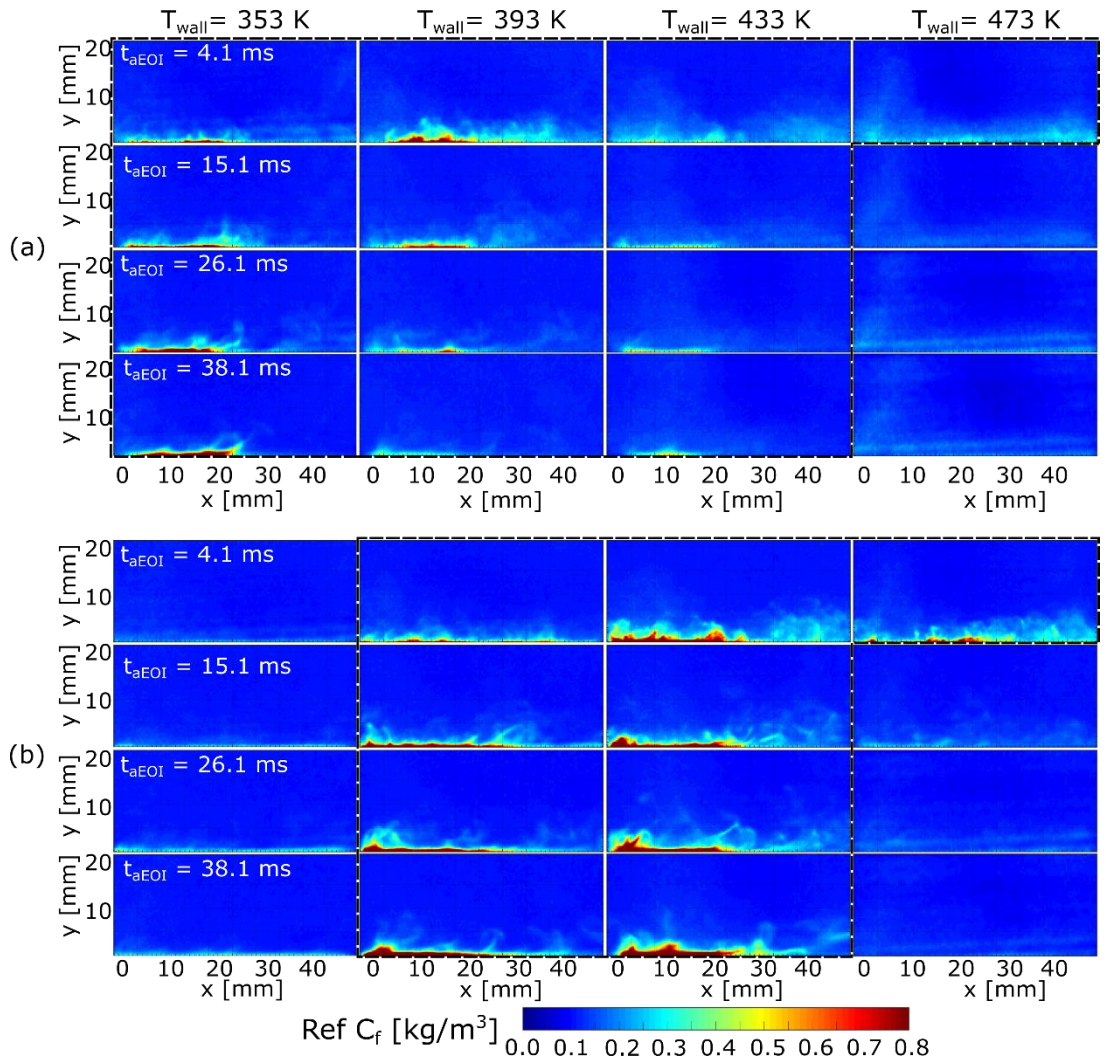

Figure 4. 2D Maps of concentration (C_f) for the pDFB (a) and 1-MN (b) under four wall temperatures and different acquisition times at $P_{inj} = 200\ bar$. A dashed line indicates the conditions with higher vaporization. (The vapor concentration were equal to or greater than 0.475kg/m^3).

2.3 CCD characterization

In this section, the link between the vaporization process and combustion chamber deposit is established. SEM images, pictures of the distribution of deposits, at $P_{inj} = 30\ bar$, and the deposit build-up rate for all the tested conditions are presented in Figure 5. Each point in the curve corresponds to almost 450 cycles. The SEM images correspond to the right side of impingement region, which was marked by a yellow mark in Figure 5b. Analyzing the SEM images, it is possible to see structures that are similar in shape to those found inside a hole injector [30]. Globular smooth structures of deposits are found at the lowest temperature. Their morphology underwent an irregular deformation characterized by small ball-like shapes when the temperature rose to 393 and 433 K. When the plate was maintained at 473 K fractal

aggregates and fractal terminations (coral shaped), characteristic of pyrolysis on injectors, were observed.

As observed in Figure 5c, the peak for build-up rate at the different conditions was found at 393 K. This could be explained by the chemical behavior of the components that were retained on the impingement region and not just by the quantity of fuel retained. The results obtained from Mie and Schlieren measurements showed an intermediate behavior at 393 K for 100 and 200 bar; Figure 3 shows this behavior for the latter pressure. This behavior can be associated with the temperature range where higher vaporization takes place in the distillation curve, around 363 and 393 K (Figure 1). Under those conditions, the liquid that settles on the surface was mainly composed of the heavy fraction. The 2T-LIF results confirmed this observation and indicated that before 433 K, a high quantity of the heavy fraction was retained on the fuel film (Figure 4).

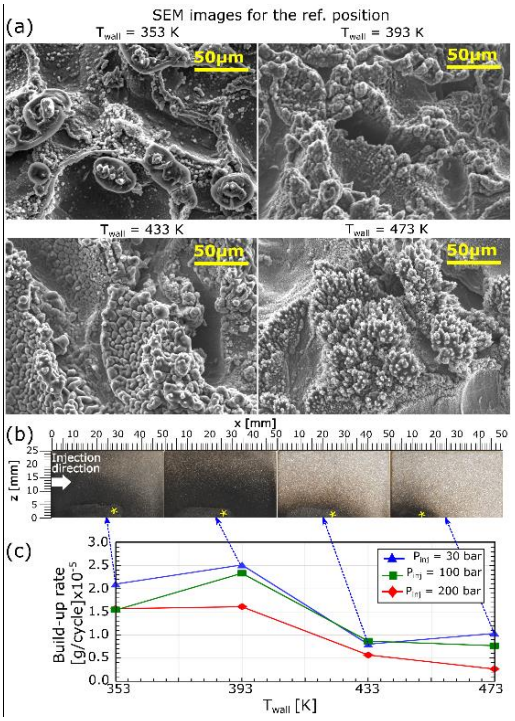

Figure 5. Deposit build up rate at different injection pressures: 30, 100, and 200 bar. Each point was obtained after almost 500 reactive cycles. SEM images (a) for the reference position (yellow stars) indicated on the plate surface pictures (b) were added at $P_{inj} = 30\ bar$.

The lowest temperature (353 K) did not produce the highest quantity of CCD because apparently there was an interference of the light fraction when the flame interacted with the fuel film or during the pyrolysis process inside the pool fires, which induced a better burning of the heavy fraction retained

[13]. However, when the light fraction is almost completely vaporized (at 393 K) leaving the heavy fraction on the impingement region, this situation can generate a favorable condition for soot and CCD generation. The heavy fraction in the case of the reference fuel was represented by 1-MN, which is considered as a generator of soot and CCD [8–11]. When the wall temperature was increased to 433K, the heavy fraction reached its maximum vaporization. This, added to some convective mechanism of mass transfer due to the temperature gradient between the plate and ambient, can improve its burning during the fuel-film-flame interaction, thus reducing the soot and CCD. At 473 K, the almost complete vaporization of the fuel components reduced the CCD build-up rate. The same trend was observed for all P_{inj}. Though the behavior at 200 bar was slightly different, this can be more associated with the quantity of heavy fraction retained on the impingement region, which was reduced when the pressure was increased.

The peak of build-up rate followed the trend of soot production presented in previous studies [22,23]. The soot production was linked directly to the quantity of CCD produced with the reference fuel because their highest production occurred at 393K. As a result of the high production of soot, the probability of its being deposited on the surface increases. This results in a higher build-up of deposits on the surface through mechanisms such as sticking, incorporation or impact [15].

As per the above discussion, the main driver responsible for CCD build-up rate was the presence of a large quantity of the heavy fraction retained on the impingement region, which promoted the generation of pool fires under an environment favorable to pyrolysis reactions on the fuel film. However, scanning electron microscope (SEM) observations on the profile of the CCD revealed that the highest quantity of deposit was found outside and next to the impingement region. This CCD distribution could be explained by the presence of a convective mechanism during combustion, such as entrainment flows, which can drive the products of the pool fires from the impingement region to its near surroundings.

3. Conclusions

Three different approximations were adapted to deduce the effect of the fuel vaporization on the CCD under four T_{wall} and three P_{inj}. The analysis involved non-reactive and reactive conditions inside a

CVCC. Two fuels with similar vaporization behavior were used during the experiments to avoid interferences between techniques. From the experiments and analysis, the following conclusions can be drawn:

- The results of the Mie scattering and Schlieren measurements showed a faster vaporization when the injection pressure rose up to 200 bar, which was improved when the wall temperature was increased.
- The 2T-LIF measurements showed that the main driver of the increase in the CCD build-up rate was the heavy fraction. The chemical characteristics of the heavy fraction could have more impact than its retained quantity on soot and CCD generated during the combustion. In addition, the possible influence of the presence of the light fraction at the lowest temperature (353 K) could reduce the production of CCD.
- The distribution of the CCD indicated that they were located mainly outside the impingement region. This can be explained by the entrainment flows that developed during the combustion process.

Acknowledgments

Financial support from Continental Powertrain (USA) and Central-Val de Loiret Region (France) is gratefully acknowledged.

References

[1] US Enviromental Protection Agency, Light-Duty Automotive Technology, Carbon Dioxide Emissions, and Fuel Economy Trends: 1975 Through 2017, Technical report, 2018, available at: htpps://www.epa.gov/automotive-trends.

[2] The International Council on Clean Transportation, European vehicle market statistics 2017/2018, Technical report, 2018, available at https://theicct.org/publications/European-vehicle-market-statistics-20172018.

[3] M. Bardi, A. Di Lella, G. Bruneaux, A novel approach for quantitative measurements of preferential evaporation of fuel by means of two-tracer laser induced fluorescence, Fuel 239(2019):521–533.

[4] J. Senda, T. Higaki, Y. Sagane, H. Fujimoto, Y. Takagi, M., Adachi, Modeling and measurement on evaporation process of multicomponent fuels, SAE Tech. Pap. (2000) 2000-01-0280.

[5] J. Senda, H. Fujimoto, Multicomponent Fuel Consideration for Spray Evaporation Field and Spray-Wall Interaction, SAE Tech. Pap. (2001) 2001-01-1071.

[6] D. Kawano, J. Senda, Y. Wada, H. Fujimoto, Y. Goto, M. Odaka, H. Ishii, H. Suzuki, Numerical Simulation of Multicomponent Fuel Spray, , SAE Tech. Pap. (2003) 2003-01-1838.

[7] J.K. Yoon, K.J., Myong, J. Senda, H. Fujimoto, Analysis of spatial vapor-phase distribution using the LIF method on multi-component fuel, J. Mech. Sci. Technol. 23(9)(2009)2565–2573.

[8] M. Fatouraie, M. Frommherz, M. Mosburger, E. Chapman, S. Li, R. McCormick, G. Fioroni, Investigation of the Impact of Fuel Properties on Particulate Number Emission of a Modern Gasoline Direct Injection Engine, SAE Tech. Pap. (2018) 2018-01-0358.

[9] Y. Kobayashi, M. Arai, Characteristics of PM Exhausted from Pool Diffusion Flame with Gasoline and Surrogate Gasoline Fuels, SAE Int. J. Engines 9(1)(2016)315-321.
[10] P.J. Choate, J.C. Edwards, Relationship Between Combustion Chamber Deposits, Fuel Composition, and Combustion Chamber Deposit Structure, SAE Tech. Pap. (1993) 932812.
[11] T. Uehara, Y. Takei, H. Hoshi, K. Shiratani, M. Okada, Y. Esaki, Study on Combustion Chamber Deposit Formation Mechanism Influence of Fuel Components and Gasoline Detergents, SAE Tech. Pap. (1997) 971722.
[12] H. Sandquist, I. Denbratt, F. Owrang, J. Olsson, Influence of Fuel Parameters on Deposit Formation and Emissions in a Direct Injection Stratified Charge SI Engine, SAE Tech. Pap. (2001) 2001-01-2028.
[13] I. A. Khalek, T. Bougher, T., J. J. Jetter, Particle emissions from a 2009 gasoline direct injection engine using different commercially available fuels, SAE Int. J. Fuels Lubr. 3(2) (2010) 623–637.
[14] L. Ganeau, M.A. Fortunato, G. Pilla, G. Bruneaux, C. Schulz, A New Methodology to Study the Mechanisms of Combustion-Chamber Deposit Formation and the Effects of Engine Parameters on the Quantity and Morphology of Combustion-Chamber Deposits, JSAE(2019) 2019-01-2355.
[15] G. Lepperhoff, M. Houben, Mechanisms of Deposit Formation in Internal Combustion Engines and Heat Exchangers, SAE Tech. Pap. (1993) 931032.
[16] G.T. Kalghatgi, Combustion Chamber Deposits in Spark-Ignition Engines: A Literature Review, SAE Tech. Pap. (1995) 952443.
[17] Y. Li, H. Zhao, B. Leach, T. Ma, N. Ladommatos, In-Cylinder Measurements of Fuel Stratification in a Twin-Spark Three-Valve SI Engine, SAE Tech. Pap. (2004) 2004-01-1354.
[18] I. Lama, G. Bruneaux, A. Di, Lella, C., Schulz, Two-tracer LIF imaging of preferential evaporation of multi-component gasoline fuel sprays under engine conditions, Proc. Combust. Inst. 35(3) (2015) 2915–2922.
[19] W.J. Pitz, N.P. Cernansky, F.L. Dryer, F.N. Egolfopoulos, J.T. Farrell, D.G. Friend, H. Pitsch, Development of an experimental database and chemical kinetic models for surrogate gasoline fuels, SAE Tech. Pap. (2007) 2007-01-0175.
[20] L. Cai, H. Pitsch, Optimized chemical mechanism for combustion of gasoline surrogate fuels, Combust. Flame 162(5) (2015)1623–1637.
[21] B. Galmiche, Caractérisation expérimentale des flammes laminaires et turbulentes en expansion, PhD Thesis, Université d'Orléans, France, 2014.
[22] A. Roque, F. Foucher, W. Imoehl, J. Helie, Generation and Oxidation of Soot Due to Fuel Films Utilizing High Speed Visualization Techniques, SAE Tech. Pap. (2019) 2019-01-0251.
[23] A. Roque, F. Foucher, Q. Lamiel, B. Imoehl, N. Lamarque, and J. Helie, Impact of gasoline direct injection fuel films on exhaust soot production in a model experiment, Int. J. Engine Res. (2019) 1-24.
[24] Q. Lamiel, Analysis of spray-wall impingement, fuel film spreading and vaporisation for reciprocating engine applications., PhD Thesis, Universite de Toulouse, France, 2019.
[25] B.L. Smith, T.J. Bruno, Improvements in the measurement of distillation curves: Application to gasoline and gasoline + methanol mixtures, Ind. Eng. Chem. Res. 46(1) (2007)297–309.
[26] A. Montanaro, L. Allocca, G. Meccariello, M. Lazzaro, Schlieren and Mie Scattering Imaging System to Evaluate Liquid and Vapor Contours of a Gasoline Spray Impacting on a Heated Wall, SAE Tech. Pap. (2015), 2015-24-2473.
[27] A. Montanaro, L. Allocca, M. Lazzaro, G. Meccariello, Impinging Jets of Fuel on a Heated Surface: Effects of Wall Temperature and Injection Conditions, SAE Tech. Pap. (2016) 2016-01-0863.
[28] R. Gonzalez, R. Woods, S. Eddins, Digital Image Processing Using MATLAB, 2nd ed., Gatesmark Publishing,USA, 2009.

[29] P. Kranz, S.A. Kaiser, LIF-based imaging of preferential evaporation of a multi-component gasoline surrogate in a direct-injection engine, Proc. Combust. Inst. 37(2)(2019)1365–1372.
[30] J. Barker, J. Reid, S. Mulqueen, G.J. Langley, E.MJ. Wilmot, S. Vadodaria, J. Castle, J. Whitaker, The Investigation of the Structure and Origins of Gasoline Direct Injection (GDI) Deposits, JSAE (2019) 2019-01-2356.